The International Journal of Materials and Engineering Technology (TIJMET) (2023) 6(1)
http://dergipark.gov.tr/tijmet
ISSN: 2667-4033

RESEARCH ARTICLE

An approach on determining micro-strain and crystallite size values of thermal spray barrier coated Inconel 601 super alloy

Nida Nur Erdoğan*[1], Aziz Barış Başyiğit[2]

[1]Kırıkkale University, Institute of Science, Department of Mechanical Engineering, Kırıkkale, Türkiye
[2]Kırıkkale University, Faculty of Engineering and Architecture, Department of Metallurgical and Material Engineering, Kırıkkale, Türkiye

Article Info

Article history:
Received: 05.06.2023
Revised:21.06.2023
Accepted:30.06.2023
Published Online: 30.06.2023

Keywords:
Thermal barrier coatings
Inconel 601 alloy
Micro-strain analyze
Crystallite size

Abstract

Iron-based, nickel-based, and cobalt-based superalloys are the three types of superalloys utilized in high-temperature applications. Inconel 601 is a nickel-based superalloy that's used especially in aerospace, heat treatment, and gas turbine engine applications. In this study, thermal barrier coating (TBC) was applied approximately at 100, 200 and 300 µm ceramic top coating thicknesses and X-Ray Diffraction (XRD) analyzes were performed. NiCrAlY metallic powder was used for bond coating and 8% YSZ ceramic powder was used for ceramic top coating. Crystallite sizes and micro-strain values were calculated with the Scherrer Equation, Williamson-Hall method and Modified Scherrer (Monshi-Scherrer) equation of the compounds obtained at the peak points in XRD analysis.

1. Introduction

Super-alloys are used in high-temperature applications because of their satisfactory mechanical strength, stability, and resistance to wear and corrosion. They are classified into three major classes based on their nickel, iron, and cobalt content [1]. Nickel-based super-alloys can be efficiently produced by alloying with elements such as chromium, and/or aluminum in a face centered cubic nickel matrix [2]. Nickel-based super-alloys have a nickel content of 30-75% and a chromium content of up to 30% by weight. Furthermore, some alloying elements such as titanium, cobalt, boron, zirconium, and carbon are also added to their compositions [3]. In applications where very high temperatures are present, such as jet engines, aviation vehicle parts, and industrial heaters, Inconel 601 alloy is also preferred. The face-centered cubic (FCC) gamma phase, carbides and borides, delta and sigma phases, and other topologically close-packed structures in the microstructure of super-alloys increase the alloy's strength and provide resistance to corrosion and oxidation [4,5].

Whether the mechanical properties, wear and corrosion resistance of super alloys is insufficient, the requisite properties can be achieved by subjecting these materials to heat treatment and coating methods. It is anticipated that when service life is enhanced and performance standards rise, there will be more usage fields for super alloys. Diffusion and overlay coating, thermal barrier coating are the three types of surface hardening techniques used on super-alloys. While diffusion coating and overlay coating methods are primarily used to protect materials from abrasion, oxidation, and corrosion, thermal barrier coating processes are used to shield materials from high ranges of heat [4].

Stress relief annealing, full annealing, diffusion coating and age hardening are the four heat treatments that are most frequently used on super-alloys [6,7]. By preventing creep, thermal barrier coatings (TBC) are used to lower oxidation rates and heat flow in materials. These systems are mostly used in aircrafts and gas turbines. TBCs are made up of a bond coat, a thermally generated oxide (TGO), and a ceramic top coat [8,9].

Crystallite size is frequently determined in monodisperse microstructures using X-ray diffraction patterns and other experimental approaches such as transmission electron microscopy. Dislocations are prevented from moving freely throughout a material by grain boundaries. The stress field of the grain boundary defect zone, which is typically aligned along the boundaries, prevents dislocation from propagating. Therefore, one popular method of boosting strength is to reduce the grain size. The Hall-Petch connection provides the size-force relationship for crystallites. Grain boundaries are the favored locations for the beginning of corrosion and the precipitation of new phases from solids due to their high interfacial energy and relatively weak bonding [10-11].

Studies for various substrate materials and coatings are also intriguing, even though there are no studies for superalloys in the literature. Mateus D.F.A. et. al., throughout the thickness of the titanium nitride thin films, the crystallite size and micro-strain were examined. For two different thicknesses, the films were deposited onto 316 stainless steel substrates using the Plasma Assisted Physical Vapor Deposition process (PAPVD). The crystallite size and microstrain as a function of film depth were examined for the (111) and (200) orientations. Both films exhibit anisotropic behavior, according to the results [12]. Augustin A. et.al., discovered that the crystallite size in electrodeposited copper plating fluctuates with deposition current density, and they evaluated the crystallite size and micro-strain in the plating using the Williamson-Hall method. The values of crystallite sizes obtained from TEM micrographs were found to be consistent with those obtained from the Williamson-Hall method. The existence of nano-twins in the coating also contributed to the copper coating's micro-strains [13]. Pilliadugula R. et.al., The XRD pattern of beta-Ga2O3 powder, synthesized at low temperature using a template-free two-step hydrothermal process, is fully examined using several methods

Corresponding Author: Nida Nur Erdoğan
E-mail: nida.erdogaan@gmail.com

How to cite this article:
Erdoğan, N.N., Başyiğit, A.B., An approach on determining micro-strain and crystallite size values of thermal spray barrier coated Inconel 601 super alloy, The International Journal of Materials and Engineering Technology (TIJMET), 2023, 6(1):21-25

of analysis. The crystallite sizes as well as the micro-strains of the micro-structures are studied and compared. For the inquiry, in addition to the classic Scherrer's formula (S-average, LF, and LFTZ), the modified Williamson-Hall (W-H) approach with UDM, USDM, and UDEDM, and the Size-Strain Plot (SSP) method were used. It was discovered that the crystallite sizes generated from the UDM modified W-H analysis and SSP models closely matched the crystallite sizes observed in the TEM micrograph [14].

In this study, Thermal barrier coating method was applied on Inconel 601 samples approximately at 100, 200 and 300 µm ceramic top coating thicknesses and XRD analyzes were performed. Crystallite sizes and microstrain values of 100, 200, 300 µm 8% YSZ TBC coated Inconel 601 samples were calculated by Scherrer, Monshi Scherrer and Williamson-Hall methods.Scherrer equation is a formula in XRD and X-Ray Crystallography that relates the size of submicron crystallites in a solid to the broadening of a peak in the diffraction pattern. The Williamson-Hall analysis is that the expansion is functions of the peak width if it is both size-induced and strain-induced.

2. Materials and methods

The Inconel 601 experimental material used in the study is constructed of circular bars measuring 16 mm in diameter by 400 mm in length that have been lightly cold rolled to obtain a clean finish. Wire erosion was used to cut this material to prepare 4 samples per each case depth in dimensions of Ø16x7 mm.

The chemical composition of the Inconel 601 raw material in the study was determined using an argon optical spectrometer of the Amatex brand and Spectromaxx model. The Inconel 601 alloy's average chemical composition was obtained and is shown in Table 1.

Table 1. The chemical composition of Inconel 601

Element	Chemical composition (%wt)
Ni	58,225
Cr	23,000
Fe	16,375
Al	1,000
C	0,100
Mn	0,320
Si	0,430
Cu	0,034
Others	0,516

For thermal barrier coating process, initially, samples were cleaned using sandblasting. The samples were then put inside the coating device. On the Inconel 601 experimental material, NiCrAlY powder was applied as the bond coat material using the HVOF spray method, and 8% YSZ was coated as the ceramic top coat material over the bond coat using the APS method.

The scanning angle range used for XRD (X-Ray Diffraction) analysis was 10-90°, and the scanning speed was set to 2 deg/min. A Rigaku Ultima IV X-ray diffractometer with a copper-targeted X-ray tube and operating voltage and current settings of 40 kV and 30 mA was used for the analysis.

3. Results and discussion

Sample 1 represents 100 µm, sample 2 represents 200 µm, sample 3 represents 300 µm ceramic top coated samples and sample 4 represents Inconel 601 raw material. Fig.1. shows the XRD datas of sample 1, sample 2, sample 3 and sample 4. The letter t represents the tetragonal structure and the letter c represents the cubic structure. The lattice parameters and crystal systems given in the Table.2 were found through the X-Pert Highscore Plus software.

Table 2. Lattice parameters and crystal systems of compounds obtained from XRD datas

Compounds	Lattice parameters			Crystal Systems
	a (Å)	b (Å)	c (Å)	
$Y_{0.19}Zr_{1.81}O_{3.9}$	3,616	3,616	5,158	t
$O_{3.87}Zr_{1.74}Y_{0.26}$	3,625	3,625	5,14	t
ZrO_2	5,129	5,129	5,129	c
$Ni_{2.88}W_{0.32}Cr_{0.8}$	3,573	3,573	3,573	c
Ni_4	3,571	3,571	3,571	c
CrNi	3,591	3,591	3,591	c
Fe_4	3,49	3,49	3,49	c

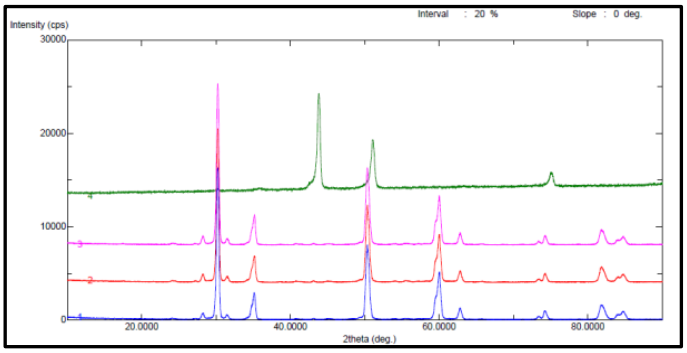

Figure 1. XRD data of Sample 1, Sample 2, Sample 3 and Sample 4

- Analyzing the XRD results of Sample 1's, at 30.2º, 35.2º, 50.3º, 62.8º, 74.2º, 81.8º, and 84.7º from the (101), (110), (112), (211), (202), (220), (213) and (310) planes of $Y_{0.19}Zr_{1.81}O_{3.9}$ in tetragonal structure,
- Analyzing the XRD results of Sample 2's, at 30,2˚, 35˚, 50,3˚, 59,8˚, 62,7˚, 73,9˚, 81,8˚ and 84,5˚ from the (101), (110), (112), (211), (202), (220), (213) and (310) planes of $O_{3.87}Zr_{1.74}Y_{0.26}$ in tetragonal structure and from the (111), (020), (022), (131), (222), (040), (133), (042) planes of ZrO_2 in cubic structure,
- Analyzing the XRD results of Sample 3's, at 30,2˚, 35,1˚, 50,2˚, 59,9˚, 62,7˚, 74,1˚, 81,7˚ and 84,7˚ from the (101), (110), (112), (211), (202), (220), (213) and (310) planes of $Y_{0.19}Zr_{1.81}O_{3.90}$ in tetragonal structure and from the (111), (020), (022), (131), (222), (040), (133), (042) planes of ZrO_2 in cubic structure,
- Analyzing the XRD results of Sample 4's, at 43,9˚, 51,1˚ and 75,2˚ from the (111), (200) ve (220) planes of $Ni_{2.88}W_{0.32}Cr_{0.8}$, Ni_4, CrNi and Fe_4

diffraction was recorded. Studies that are similar to this one [15–17] support these findings.

Above 2370 °C, zirconia is cubic, tetragonal between 2370 °C and 1170 °C, and monoclinic below 1170 °C [18]. Cubic ZrO_2 diffraction is clearly observed in samples with ceramic top coating thicknesses of 200 and 300 µm. The cooling of the

samples at room temperature following the process, which varies depending on the TBC processing temperature and coating thickness is expected to have an effect on the visual cubic structure of the zirconia.

The raw Inconel 601 sample (Sample 4) had CrNi and $Ni_{2.88}W_{0.32}Cr_{0.8}$ diffractions, as well as cubic Ni_4 and Fe_4 structures, as predicted. The Ni matrix, clearly generate bonds with the alloying elements W and Cr.

3.1. Calculation of Crystallite Sizes, Strain Density and Micro-Strain Values with Scherrer Equation

Scherrer equation is a formula in XRD and X-Ray Crystallography that relates the size of submicron crystallites in a solid to the broadening of a peak in the diffraction pattern.

The Scherrer equation, used in both X-ray crystallography and X-ray diffractometery, relates the size of submicron crystallites in Equation (1), where D is the nanocrystal size, K is the shape factor, typically taken to be 0.89 for ceramic materials is the wavelength of radiation in nanometers, is the diffracted angle of the peak, and is the full width at half maximum of the peak in radians [19,20].

$$D = \frac{K.\lambda}{\beta.\cos\theta} \quad (1)$$

Crystallite sizes calculated using the Scherrer equation Table.3 has been given.

Table 3. Crystallite sizes

Peak No	Sample 1	Sample 2	Sample 3	Sample 4
	Crystallite sizes (nm)			
1	21,3	21,3	21,3	22,2
2	27,1	27,2	31,1	17,5
3	18,9	14,1	20,7	18,5
4	26,5	23,8	26,5	-
5	17,1	17,1	20,1	-
6	21,5	21,5	21,5	-
7	11,2	16,9	11,2	-
8	17,3	17,3	15,4	-

When the crystallite sizes calculated from XRD peak points with Scherrer's equation are examined, the mean crystallite size for Sample 1 is 20.1 nm, the mean crystallite size for sample 2 is 19.9 nm, the mean crystallite size for sample 3 is 20.98, and the mean crystal size for sample 4 is 19.4 nm. The formulas and explanations of D, δ and ε are given below.
D = crystallite size,

$$\delta = \delta = \frac{1}{D^2} \text{ strain density,} \quad (2)$$

$$\varepsilon = \frac{\beta}{4\tan\theta} \text{ microstrain [17,18].} \quad (3)$$

When δ and ε values are calculated for the major peak points of the samples,

- For Sample 1, $\delta = 2.204 \times 10^{-3}$ nm^{-2} , $\varepsilon = 6 \times 10^{-3}$,
- For Sample 2, $\delta = 2.204 \times 10^{-3}$ nm^{-2} , $\varepsilon = 5.9 \times 10^{-3}$,
- For Sample 3 $\delta = 2.204 \times 10^{-3}$ nm^{-2}, $\varepsilon = 5.92 \times 10^{-3}$,
- For Sample 4, $\delta = 2.03 \times 10^{-3}$ nm^{-2} , $\varepsilon = 4.67 \times 10^{-3}$ are found.

3.2. Calculation of Micro-Strain Values by Williamson-Hall (UDM) Method

The Williamson-Hall method, on the other hand, assumes that the broadening of the peaks is the cumulative effect of size-induced expansion and strain-induced expansion. William-Hall method; It can be expressed as $\beta_{total} = \beta_{size} + \beta_{strain}$. Uniform deformation model (UDM), also known as the modified W-H method;

$$\varepsilon = \frac{\beta}{4.\tan\theta} = \beta_{strain} . \frac{\cos\theta}{4.\sin\theta} \quad (4)$$

$$\beta_{total} = \beta_{size} + \beta_{strain} = \frac{K.\lambda}{D.\cos\theta} + 4\varepsilon\frac{\sin\theta}{\cos\theta} \quad (5)$$

$$\beta_{total}.\cos\theta = \frac{K.\lambda}{D} + 4\varepsilon\sin\theta \quad (6)$$

can be expressed [20]. According to the Williamson-Hall (UDM) method, the equation expressed in Equation specifies a line whose slope is ε and the point where it intersects the y-axis is $\frac{K.\lambda}{D}$. Figure 2 shows Williamson Hall (UDM) plots with the peak values of the samples.

The slope of the Williamson-Hall plots plotted with the values of the peak points of the samples, hence the total microstrain values from the size and deformation of the samples, are $0{,}39\text{x}10^{-3}$, $0{,}13\text{x}10^{-3}$, $0{,}29\text{x}10^{-4}$ and $-0{,}26\text{x}10^{-3}$ respectively. It is positive values indicate that microstrain is under the influence of tensile stress, while negative values indicate that it is under the influence of compressive stress.

3.3. Calculation of Crystallite Sizes with Modified Scherrer (Monshi – Scherrer) Equation

The premise of the modified Scherrer formula is that, by applying the least squares approach to mathematically reduce the source of mistakes, reduce errors and obtain the average value of L via all peaks. The Monshi-Scherrer equation is expressed below. Taking the logarithm of both sides of the Scherrer equation;

$$\ln\beta = \ln\frac{K.\lambda}{D.\cos\theta} = \ln\frac{K.\lambda}{D} + \ln\frac{1}{\cos\theta} \quad (7)$$

A straight line with an intercept of around lnK/L and a slope of about one must be obtained if the results of ln versus ln(1/cosθ) are plotted. Since tan45° = 1, this line should theoretically have a slope of 45°. The least squares method, however, provides the best slope and most accurate lnK/L because mistakes are linked to experimental data [21].

The intercept is first obtained, and then the exponential of t he intercept is found as;

$$e^{intercept} = \frac{K.\lambda}{D} \quad (8)$$

Figure 3 shows Monschi-Scherrer plots plotted with the peak values of the samples.

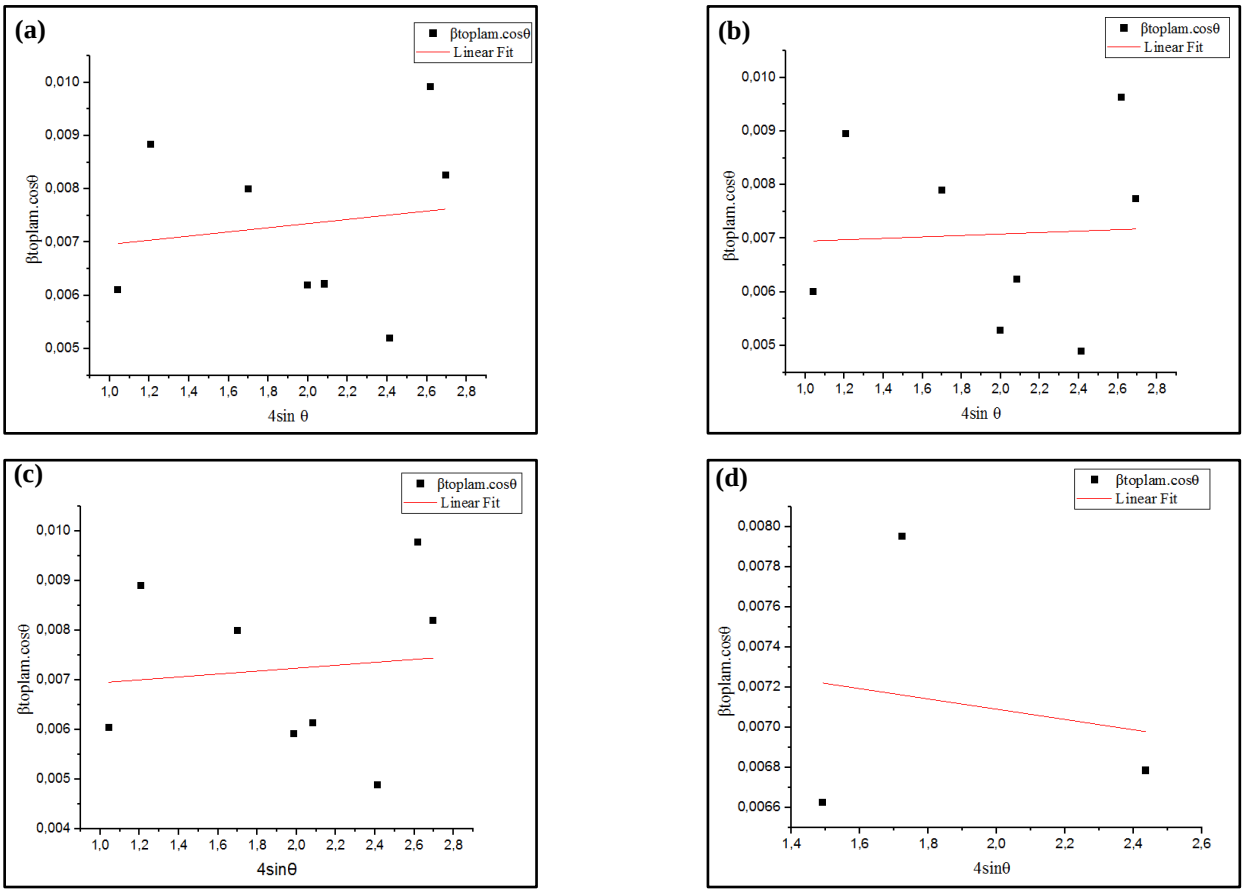

Figure 2. Williamson Hall (UDM) plots plotted with the peak values of the samples. (a) Sample 1 (b) Sample 2 (c) Sample 3 (d) Sample 4

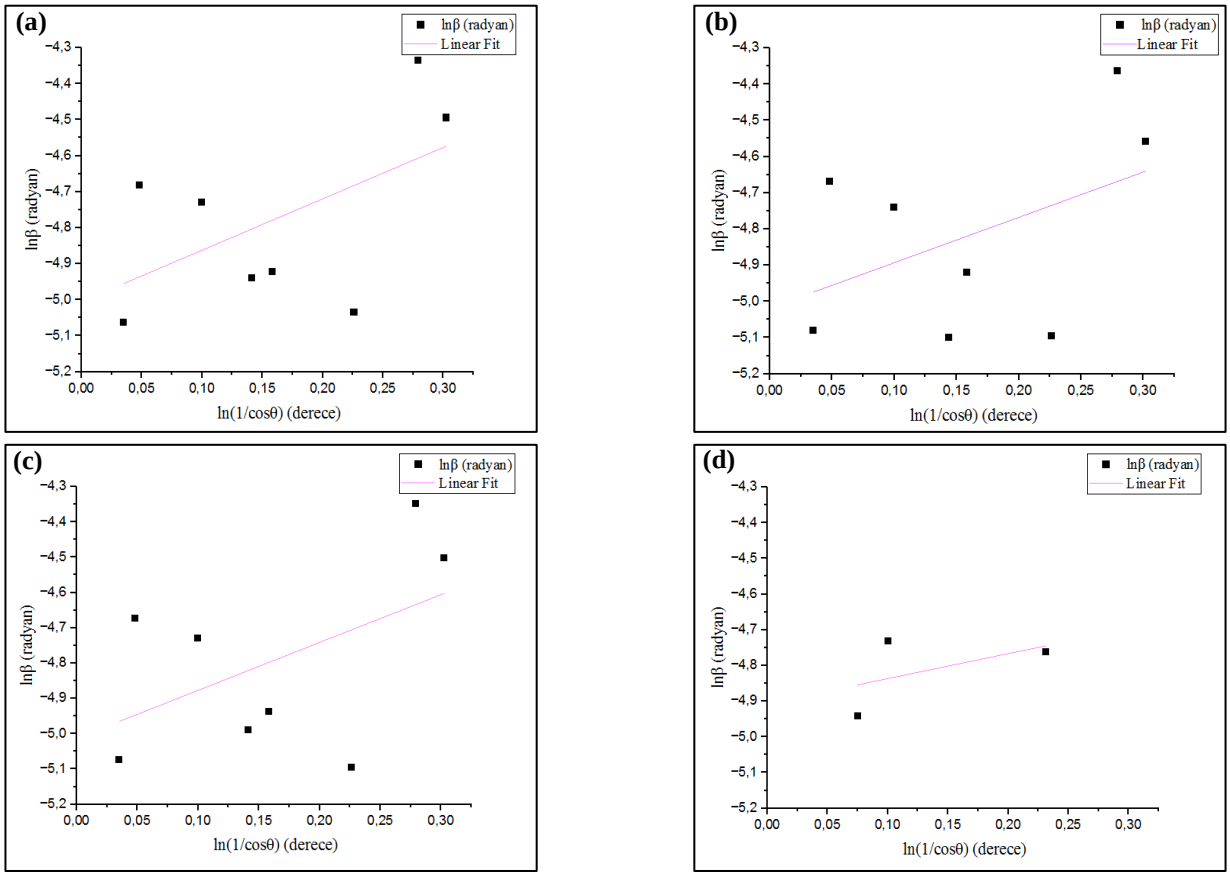

Figure 3. Monschi-Scherrer plots plotted with the peak values of the samples. (a) Sample 1 (b) Sample 2 (c) Sample 3 (d) Sample 4

It is seen that the points where the Monschi-Scherrer graph drawn for Sample 1, Sample 2, Sample 3 and Sample 4 intersect the y-axis are -5,00515, -5,01819, -5,01257 and -4,90664, respectively.

When the $e^{intercept} = \frac{K.\lambda}{D}$ equations are met, the crystallite sizes of the samples found by the Monschi-Scherrer equation are 21,6, 21,9, 24,4 and 19,6 nm, respectively.

4. Conclusions

As a result, crystallite sizes and micro-strain values of coatings and raw Inconel 601 super-alloy were calculated by XRD patterns applied to 100, 200 and 300 micron TBC coated with 8% YSZ powder on experimental material Inconel 601. Accordingly, the crystallite sizes obtained by Scherrer's equation were calculated as 20,1 nm, 19,9 nm, 20,98 nm, 19,4 nm for 100,200,300 μm ceramic top-coated and Inconel 601 samples, respectively. The crystallite sizes obtained by the modified Monshi-Scherrer equation are 21,6, 21,9, 24,4 and 19,6 nm, respectively. The microstrain values obtained by Williamson-Hall method are; $0{,}39x10^{-3}$, $0{,}13x10^{-3}$, $0{,}29x10^{-4}$ and $-0{,}26x10^{-3}$ respectively. This is because Williamson-Hall analysis, both size-induced and strain-induced Scherrer equation are functions of the peak width of the size-induced expansion only. However, the results obtained by these two distinct methods are highly correlated and will show the same trends as the synthesis conditions change. Although the Williamson-Hall method makes a lot of assumptions, it can be useful when applied in a relative sense. For instance, a study of numerous powder patterns of the same chemical compound synthesized under various conditions may reveal trends in crystallite size and strain. Based on the results, material strength will be stronger with lower particle sizes computed using the Scherrer equation, and hence smaller grain size. Nonetheless, the experiment can be repeated and the findings compared for various superalloy compositions and coatings.

Acknowledgments

Authors would like to thank Kırıkkale University Scientific Research Projects Department for financial supports (Project Code: 2022/053).

Author contributions

N. N. Erdoğan: Conceptualization, Data curation, Formal analysis, Funding acquisition, Investigation, Resources, Software, Visualization, Roles/Writing - original draft, Review & editing

A.B.Başyiğit: Conceptualization, Data curation, Formal analysis, Funding acquisition, Investigation, Methodology, Project administration, Resources, Supervision, Validation, Roles/Writing - original draft, Review & editing

References

1. Çay, V.V., Ozan, S., Süperalaşımlar ve Uygulama Alanları, Doğu Anadolu Bölgesi Araştırmaları, **2005**, 3(2):178-188
2. Akça, E., Gürsel, A., A Review on Superalloys and IN718 Nickel-Based Inconel Superalloy, Periodicals of Engineering and Natural Sciences, **2015**, 3(1)
3. Atmaca, E.S., Inconel 718 Süperalaşımının PVD Yöntemi ile AlTiN ve CrN Kaplanması ve Karakterize Edilmesi, Gazi Üniversitesi, Metalurji ve Malzeme Anabilim Dalı, Yüksek Lisans Tezi, Nisan **2015**
4. Reed, R.C., The Superalloys Fundamentals and Applications, Cambridge University Press, **2006**, 1-28
5. Donachie, M.J., and Donachie, S.J., Superalloys A Technical Guide, Second Edition, ASM International, **2002**, 25-39
6. Watson, J.E., Superalloys, Production, Properties and Applications, Nova Science Publishers, Inc. New York, **2011**, 25-44
7. Heubner, U., Nickel Alloys, CRC Press Taylor & Francis Group, Germany, **2018**, 129-160
8. ASM Specialty Handbook: Nickel, Cobalt, and Their Alloys, **2000**, 9-54, 287
9. Galetz, M.C., Coatings on Superalloys, Superalloys, Coatings for Superalloys, InTech, **2015**
10. Doherty, R.D., Hughes, D.A., Humphreys, F.J., Jonas, J.J., Jensen, D.J., Kassner, M.E., King, W.E., McNelley, T.R., McQueen, H.J., Rollett, A.D., Current issues in recrystallization: A review, Materials Science and Engineering: A. **1997,** 238(2):219–274
11. Allen, S., and Thomas, E., The Structure of Materials. New York: John Wiley & Sons, Inc. **1999**
12. Mateus, D., et. al., Crystallite Size and Micro-strain evolution in TiN Thin Films, Entre Ciencia E Ingenieria, WOS:000420316600007, **2011**, 9:94-106
13. Augustin, A., et. al., Crystallite Size Measurement and Micro-strain Analysis of Electrodeposited Copper Thin Film using Williamson-Hall Method, International Conference on Condensed Matter and Applied Physics, Proceedings Paper, **2016,** 1728
14. Pilliadugula, R., Gopalakrishnan, N., Crystallite size and micro-strain investigations of hydrothermally synthesized beta-Ga_2O_3 by different analytical methods, Functional Materials Letters, **2020**, 13(5)
15. Jamail, H., Razavi, R.S., Investigation of Thermal Shock Behavior of Plasma-Sprayed NiCoCrAlY/YSZ Thermal Barrier Coatings, Advanced Materials Research, **2012**, 472-475:246-250
16. Loghman-Estarki, M.R., Nejati, M., Edris, H., Razavi, R.S., Jamali, H., Pakseresht, A.H., Evaluation of hot corrosion behavior of plasma sprayed scandia and yttriaco-stabilized nanostructured thermal barrier coatings in the presence of molten sulfate and vanadate salt, Journal of the European Ceramic Society 35, **2015**, 693–702
17. Sathish, S., Geetha, M., Aruna, S.T., Balaji, N., Rajam, K.S., Asokamani, R., Studies on plasma sprayed bi-layered ceramic coating on bio-medical Ti–13Nb–13Zr alloy, Ceramics International 37, **2011**, 1333–1339
18. Kırmalı, Ö., Özdemir, A.K., Zirkonya Esaslı Seramikler, İnönü University Sağlık Bilimleri Dergisi 2, **2012**, 15-18
19. Kolhe, M.L., Karande, K.J., Deshmukh, S.G., Artificial Intelligence, Internet of Things (IOT) and Smart Materials for Energy Applications, CRC Press, **2022**, 32
20. Rabiei, M., et.al., Comparing Methods for Calculating Nanocrystal Size of Natural Hydroxyapatite Using X-Ray Diffraction, Nanomaterials **2020**, 10, 1627
21. Monshi, A., Foroughi, M.R., Monshi, M.R., Modified Scherrer Equation to Estimate More Accurately Nano-Crystallite Size Using XRD. World J. Nano Sci. Eng. **2012**, 2:154–160